Optimizing oxygen substituents of a carbon cathode for improved capacitive behavior in ethanol-based zinc-ion capacitors

YUAN Ping[1,†], XIAO Hao-ming[2,†], LI Jun-yi[2], LUO Jun-hui[2], LUO Xian-you[1], CHEN Da-ming[1,*], LI De[1,*], CHEN Yong[1,2,*]

（1. *State Key Laboratory of Marine Resource Utilization in South China Sea*, *Hainan Provincial Key Laboratory of Research on Utilization of Si-Zr-Ti Resources*, *Hainan University*, *Haikou* 570228, *China*;
2. *Guangdong Key Laboratory for Hydrogen Energy Technologies*, *School of Materials Science and Hydrogen Energy*, *Foshan University*, *Foshan* 528000, *China*）

Abstract: Zinc ion capacitors (ZICs) have been widely studied in recent years due to their high energy density, excellent rate capability, long cycling life and low cost. The incorporation of oxygen functional groups (OFGs) on the surface of the carbon-based cathodes is an effective strategy for improving the capacitive performance of aqueous ZICs. However, whether their presence helps improve the capacitance of ethanol (EtOH)-based ZICs has not been investigated. In this work, a combination of nitric acid oxidation and thermal treatment was used to regulate the OFGs on the activated surface of the carbon cathode. The optimized sample had a high specific capacitance of 195 F g^{-1} at 1 A g^{-1} using $ZnCl_2$/EtOH as the electrolyte, *i.e.*, a 56% increase compared to an unmodified cathode (125 F g^{-1}). ZICs also shown excellent stability for more than 16 000 cycles at 3 A g^{-1}, while maintaining 100% coulombic efficiency. This significantly improved performance is attributed to the presence of OFGs, especially carboxyl and ester groups, which provide abundant electrochemical active sites for redox reaction with the zinc ions. This study reports a significant improvement in the specific capacitance of carbon cathodes for commercial EtOH-based ZIC systems.

Key words: Zinc-ion capacitors; Oxygen functional groups; Ethanol; Activated carbon; Specific capacitance

1 Introduction

Electrochemical energy storage in supercapacitors, such as electric double-layer capacitors (EDLCs), can provide high power density with long cycling life[1–2]. The energy storage mechanism is based on ion adsorption/desorption at the electric double layer of electrode materials, such as activated carbon (AC)[3–4]. However, their low energy density limits large-scale practical applications[5]. Strategies to improve the energy density of EDLCs include increasing the accessible specific surface area by optimizing the pore structure and improving the electrical conductivity of AC to accelerate ion/electron transport[6–9]. The volumetric and gravimetric energy densities achieved through these strategies have reached a plateau. Therefore, new types of capacitive energy storage systems are needed to push the energy density higher.

Zinc-ion capacitors (ZICs), with metallic zinc as the anode, combine the advantages of supercapacitors and batteries, *i.e.*, high power density and high energy density, respectively, and are considered as a promising next-generation energy storage device[10–12]. Compared with lithium, sodium and potassium anodes, zinc has abundant natural resources, high chemical stability, and offers high theoretical capacity (820 mAh g^{-1})[13]. Meanwhile, zinc has a low redox potential (−0.76 V *vs.* SHE) and an outstanding two-electron reaction system[14–16]. Therefore, ZICs exhibit enormous potential as high-performance energy storage devices[17–18]. Currently, reported ZIC cathodes mainly include vanadium oxide, manganese oxide and carbon materials. Among them, porous carbons have

Received date: 2023-02-21; **Revised date:** 2023-03-23

Corresponding author: CHEN Da-ming. E-mail: chendaming@hainanu.edu.cn;
LI De. E-mail: lidenju@sina.com;
CHEN Yong, Professor. E-mail: ychen2002@163.com

Author introduction: †YUAN Ping and XIAO Hao-ming contributed equally to this work

Supplementary data associated with this article can be found in the online version.

the advantages of high specific surface area, adjustable pore structure, excellent physicochemical stability, good electrical conductivity, abundant resources, and low cost[19–22]. Introducing oxygen-containing functional groups (OFGs) has been proven to be an effective strategy to increase the pseudocapacitance of porous carbons[23–25], which can further increases the energy density of ZICs. For instance, Shuo et al.[26] demonstrated that OFGs, such as carboxyl and carbonyl groups on graphene oxide (GO), play a key role in improving the chemisorption of zinc ions and electrochemical charge storage in aqueous ZICs. Lin et al.[27] prepared GO by solvothermal method, and the specific capacitance of GO was as high as 276 F g^{-1} at 0.1 A g^{-1} in 1 mol L^{-1} H_2SO_4 electrolyte. High capacitance can be attributed to the OFGs on the carbon surface, mainly carbonyl and hydroxyl groups, leading to abundant pseudocapacitance and good wettability.

Although aqueous ZICs have received significant research attention due to their low-cost and safety, some limitations still need to be overcome, such as irreversible hydrogen evolution reaction and poor performance at low-temperature conditions. Compared with aqueous systems, organic electrolytes allow for a wider potential window, leading to improved energy density. Hu et al.[28] proposed a high-performance ZIC using $ZnCl_2$/EtOH as electrolyte, which can work at ultra-low temperatures of −78 °C and exhibit excellent cycling performance of up to 30 000 times. Compared with other organic solvents, EtOH is non-toxic, cost-effective, and allows ZICs to be installed directly under air. Furthermore, the chemical stability of EtOH inhibits side reactions and expands the voltage window. Additionally, the solvation structure $[ZnCl(EtOH)_5]^+$ formed with $ZnCl_2$ can inhibit the growth of zinc dendrites and provide good cycling stability. Therefore, ZICs based on EtOH show high energy density, wide working temperature range and easy fabrication, making this system promising for practical applications.

Since numerous studies report the positive influence of OFGs in aqueous ZICs, introducing OFGs in EtOH-based ZICs is a promising strategy to improve performance. However, this has not yet been adequately investigated. Therefore, in this study, OFGs were introduced to the surface of AC by nitric acid oxidation, and their evolution in the subsequent heat treatment and their influence on the performance of ZICs with $ZnCl_2$/EtOH electrolyte was studied. At optimum conditions, a significant capacitance increase by 56%, *i.e.*, from 125 to 195 F g^{-1} at 1 A g^{-1}, was observed. This work provides new insights into constructing OFGs on the surface of carbon materials and how they influence the performance of EtOH-based ZICs.

2 Experimental

AC was prepared from coconut shell activated by water steam, washed with 10% dilute nitric acid at 120 °C for 5 h and in deionized water to obtain neutral pH (named AC-O). Then, the obtained AC-O material was annealed at 400, 500 and 600 °C for 2 h, at a heating rate of 5 °C min^{-1} under Ar atmosphere, and the samples were denoted as AC-O-400, AC-O-500 and AC-O-600, respectively.

The specific surface area of the ACs was measured by Ar absorption at 87 K. The pore size distribution was analyzed by the quenching solid density functional theory (QSDFT) method based on a slit pore model. Scanning electron microscopy (SEM) was used to characterize the morphologies of the samples. The crystalline structures were identified by X-ray diffraction (XRD) and Raman spectroscopy. X-ray photoelectron spectroscopy (XPS) and Fourier transform infrared spectroscopy (FTIR) were executed to investigate the surface chemical compositions and oxidation states of the OFGs on the AC materials.

The cathode of ZIC was made of activated carbon, conductive carbon black and polytetrafluoroethylene in the mass ratio of 85∶10∶5 by rolling film method[28]. Then it was cut into carbon sheets with a 10 mm diameter and weighing 1.5 mg which was then pressed on carbon paper with a diameter of 12 mm under 10 MPa pressure. The anode of ZIC was

zinc foil with thickness of 20 μm and diameter of 10 mm. The electrolyte was 2 mol L^{-1} $ZnCl_2$/EtOH solution.

Cyclic voltammogram (CV) and electrochemical impedance spectroscopy (EIS) were measured on an IVIUM electrochemical workstation to evaluate the electrochemical performance. EIS was performed at a voltage amplitude of 5 mV in the frequency range of 100 kHz-0.01 Hz. The galvanostatic charging/discharging (GCD) curves were tested on a Neware battery charging/discharging system in a voltage window of 1.8 V at 3 A g^{-1}. The energy density (E) and the power density (P) of the ZICs were calculated based on the Eq. (1) and Eq. (2):

$$E = CV^2/2 \quad (1)$$

$$P = E/\Delta t \quad (2)$$

where C and V represent specific gravimetric capacitance and voltage window, respectively.

3 Results and discussion

Fig. 1a, 1b and S1 show the morphologies of the AC, AC-O-500 and AC-O samples, respectively. They exhibited similar irregular particles with large pores, indicating that the morphology of carbon was not subjected to significant change after nitric acid oxidation and thermal treatment. Some interconnected porous channels can easily be observed, which can act as reservoirs for electrolyte ions and reduce the distance between the electrode surface and ions[29–30]. The EDS mappings of AC-O-500 (Fig. 1c and d) reveal a uniform distribution of C and O, demonstrating that O was successfully retained in the sample after nitric acid and thermal treatments.

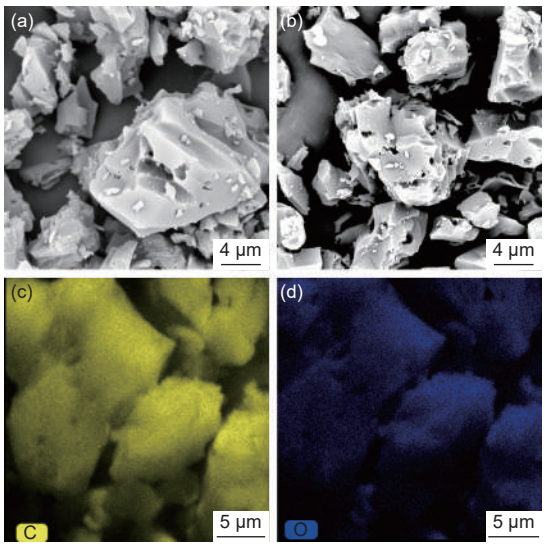

Fig. 1 SEM images of (a) AC and (b) AC-O-500. (c, d) Elemental mapping images of AC-O-500

To study the change in the specific surface areas and pore structure of the samples, Ar adsorption and desorption isotherms were measured at 87 K, as shown in Fig. 2a. All the samples exhibited type Ⅰ/Ⅳ isotherms, indicating that the ACs were mainly composed of micro- and mesopores[31]. Such porous features endow ACs with a good energy storage capacity because micropores can provide abundant active sites and mesopores are beneficial for fast ion transport[32–33]. The specific surface area of the AC-O treated with nitric acid decreased from 1 751.16 to 1 240.78 m^2 g^{-1} compared with AC (Table 1). After annealing, the specific surface area of AC-O increased slightly to 1 386.31 m^2 g^{-1} at 600 °C. As shown in Fig. 2b, the pore size distributions of AC, AC-O, AC-O-400, AC-O-500 and AC-O-600 indicate the presence of mainly micropores less than 2 nm in size. The total pore volume and micropores volume decreased when treated with nitric acid and increased slightly after annealing, indicating that the nitric acid treatment destroyed some micropores, reducing the specific surface area and pore volume. Furthermore, the introduction of excess OFGs can also block part of the pore structure, which can be explained by the increase in specific surface area and pore volume after subsequent thermal treatment reducing the oxygen content[34].

The crystal structure of AC, AC-O, AC-O-400, AC-O-500 and AC-O-600 was characterized by XRD (Fig. 2c). Diffraction peaks centered at 23° and 43° correspond to the (002) and (100) crystal planes, which are the characteristics of disordered amorphous carbon[35–36]. All the samples showed nearly identical XRD patterns, indicating that the treatment process did not change their crystal structure. Furthermore, the defects and amorphous structures of the samples were analyzed by Raman spectroscopy. As illustrated in Fig. 2d, the intensity ratio (I_D/I_G) between the D-peak

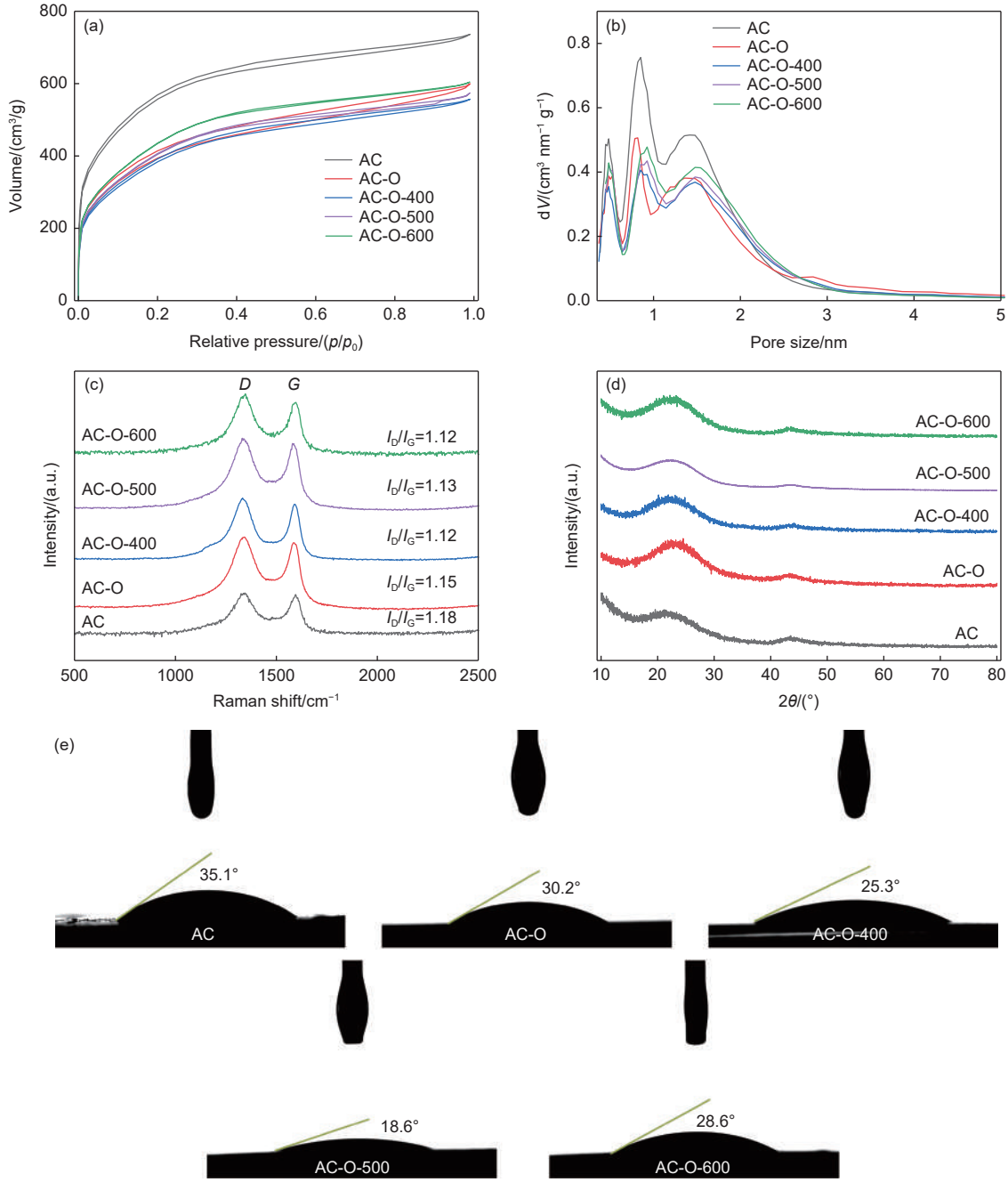

Fig. 2　(a) Ar adsorption/desorption isotherms, (b) Pore size distributions, (c) Raman spectra, (d) XRD patterns and (e) Contact angles of AC, AC-O, AC-O-400, AC-O-500 and AC-O-600

Table 1　Structural parameters of AC, AC-O, AC-O-400, AC-O-500 and AC-O-600

Samples	S_{BET}[a]/(m² g⁻¹)	S_{Micro}[b]/(m² g⁻¹)	V_{Total}[c]/(cm³ g⁻¹)	V_{Micro}[d]/(cm³ g⁻¹)
AC	1751.16	1500.97	0.904	0.734
AC-O	1240.78	1093.44	0.734	0.521
AC-O-400	1221.51	1001.25	0.684	0.498
AC-O-500	1286.62	1020.91	0.699	0.519
AC-O-600	1386.31	1086.03	0.741	0.558

Note: *a*-BET (Brunauer-Emmett-Teller) surface area. *b*-Micropore specific surface area obtained from the QSDFT method. *c*-Single-point total pore volume at $p/p_0 = 0.995$. *d*-Micropore volume obtained from the QSDFT method.

at 1 350 cm^{-1} and the *G*-peak at 1 580 cm^{-1} can describe the graphitization degree of the samples. The I_D/I_G value of the AC-O sample after nitric acid treatment was slightly lower than AC, indicating that the graphitization degree of the carbon material was improved by the oxidation treatment. The I_D/I_G value of the material remained unchanged after thermal treatment.

Contact angle measurements were conducted to investigate the surface chemistry of all samples with 2 mol L^{-1} $ZnCl_2$/EtOH electrolyte as the test droplets (Fig. 2e). The contact angles for the AC-O, AC-O-400, AC-O-500 and AC-O-600 samples were smaller than that observed with AC. AC-O-500 had the smallest contact angle of 18.6°, indicating its excellent wettability after the oxidization and heat treatment. Therefore, the introduction of OFGs elevated the surface wettability of AC materials. The improved surface wettability could lower the electrode/electrolyte interface resistance, in turn, facilitating the accessibility of zinc ions[37].

To investigate the influence of OFGs on the capacitance of the AC materials after the oxidation and thermal treatments, the electrochemical performances of AC, AC-O, AC-O-400, AC-O-500 and AC-O-600 were systematically studied by CV, GCD and EIS. As depicted in Fig. 3a, under a scan rate of 10 mV s^{-1}, a couple of obvious redox peaks can be observed, indicating the reversible redox reaction during CV tests. Compared to other samples, AC-O-500 displayed the largest integral CV area, indicating its highest specific capacitance and optimized surface functionalization. Besides, the CV curves did not exhibit significant deformation at a scan rate range of 1-100 mV s^{-1} (Fig. 3b-d), implying that the system showed fast electrochemical reaction kinetics[38]. To further explore the charge storage contribution and electrochemical kinetics behavior, the CV curves measured at different scanning rates were analyzed to distinguish the capacitive charge storage contribution and diffusion con-

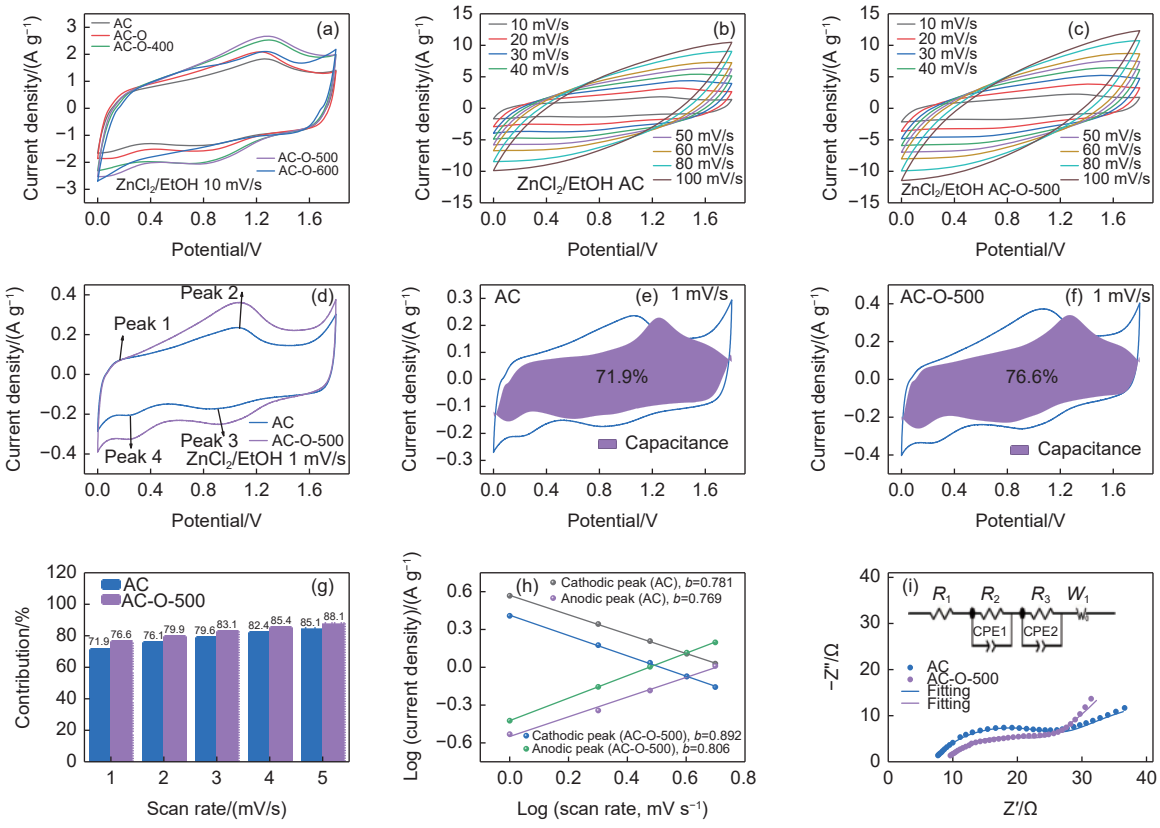

Fig. 3 (a) CV curves at different scan rates for (b) AC and (c) AC-O-500, (d) CV comparison of AC and AC-O-500 at 1 mV s^{-1}, (e, f) contribution ratio of the capacitive capacities, (g) contribution ratios, (h) *b* values in both the charge and discharge processes of AC and AC-O-500, (i) nyquist plots of AC and AC-O-500

trol charge contributions (Fig. 3e-g)[39]. When the scanning rate was 1 mV s^{-1}, the obtained result revealed that the capacitive charge contribution of AC was 71.9%, while that of AC-O-500 was 76.6%. Thus, based on the abovementioned results, AC-O-500 delivered the highest specific capacitance.

The correlation between the logarithm of current density (log *i*) and scan rate (log *v*) is shown in Fig. 3h, where the *b* value of a sample, indicative of the reaction rate, can be calculated from the slope of the trend. Here, *b* value close to 0.5 indicates slow reaction kinetics, while *b* value close to 1 corresponds to ultra-fast reaction kinetics consistent with an ideal supercapacitor[40–41]. The *b* values were found to be 0.769/0.781 for AC and 0.806/0.892 for AC-O-500. This indicates that the fast capacitance process is the main electrochemical storage mechanism of the ZIC, and the AC-O-500 electrode reveals a larger *b* value than AC, indicating its better rate performance[32].

EIS was used to characterize the electrode kinetic of ZICs (Fig. 3i), where the semicircle diameter of the high-frequency part denotes the charge transfer resistance (R_{ct}). The R_{ct} value of AC-O-500 is smaller than AC, which is mainly ascribed to the better wettability. The low-frequency region of the oblique sloping line is generally indicative of diffusion resistance. The slope of the AC-O-500 sample is larger compared to AC, indicating its smaller diffusion resistance, which is conducive to ion transport during the Zn^{2+} storage process[42]. This result also demonstrates that the introduction of OFGs can change the wettability of carbon materials and reduce resistance during the charging/discharging process.

The GCD curves of the AC and AC-O-500 samples at different rates are shown in Fig. 4a and 4b. The curves show perfect symmetry, representing the stability of the system and highly reversible Zn^{2+} plating/stripping behavior during the charge-discharge process. At 5 A g^{-1}, the IR drops for Zn//AC-O-500 and Zn//AC were 0.311 and 0.544 V, respectively, indicating AC-O-500 had a smaller internal resistance, which is consistent with the abovementioned EIS result. The rate performance of ZIC at different current densities is displayed in Fig. 4c. For AC-O-500, the specific capacitance values at 0.2, 0.5, 1, 2, 3, 4 and 5 A g^{-1} were 243, 216, 195, 176, 162, 151 and 142 F g^{-1}, respectively. These results suggest that the AC-O-500 sample had the highest specific capacitance at different current densities. At 1 A g^{-1}, the specific capacitance values of AC, AC-O, AC-O-400, AC-O-500 and AC-O-600 were 125, 143, 180, 195 and 168 F g^{-1}, respectively. AC-O-500 showed a 56% increase in specific capacitance and a significant improvement in energy density compared to pristine AC (Fig. 4d). Therefore, AC-O-500 exhibited high power density of 4 510 W kg^{-1} and excellent energy density of 64 Wh kg^{-1} (based on the mass of electrode materials). Furthermore, Fig. 4e depicts the long cycling capacity of the AC-O-500 sample. At 3 A g^{-1}, ZIC maintained 95.1% of its capacity and 100% of its coulombic efficiency after 16 000 cycles, implying excellent stability. Therefore, ZIC with an AC-O-500-based cathode can deliver an outstanding cycle life, energy density and power density, which is higher than other supercapacitors and potentially comparable to many batteries[43–48].

The surface OFGs of the oxidized and thermal treated AC samples were investigated by FTIR spectroscopy (Fig. 5a). For all samples, peaks at 1 630 and 3 440 cm^{-1} were observed, which are attributed to the in-plane vibration resulting from the presence of sp^2-hybridized C=C and C−OH, respectively[49]. The peaks centered at 1 720 and 1 460 cm^{-1} are associated with the C=O tensile vibration of the carbonyl/lactone/carboxyl groups and O−H bending vibration, respectively[50–51]. The peak at 1 080 cm^{-1} is attributed to the C−O−C tensile vibration and can be assigned to epoxides[52]. For AC-O-500, an increase in peak intensity at 1 390 cm^{-1} was observed, representing the tensile vibration of −COO[53] due to the presence of more carboxyl and ester groups on the surface. For AC-O-600, the C=O peak gradually disappeared, indicating that the high temperature resulted in the decomposition and removal of OFGs, thus reducing the reversible redox reaction and specific capacitance.

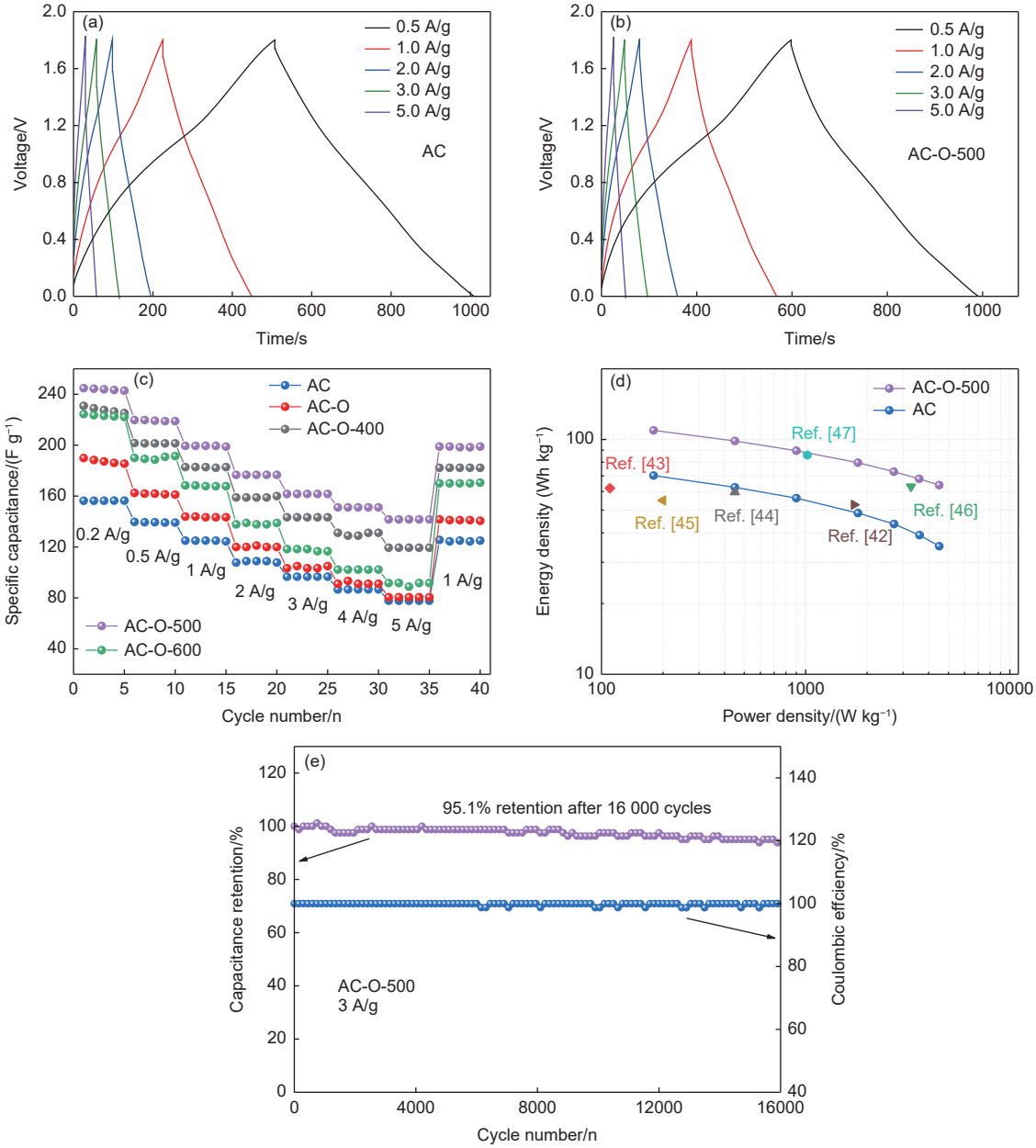

Fig. 4 GCD curves of (a) AC and (b) AC-O-500, (c) rate ability curves, (d) Ragone plot and (e) cycling stability of ZIC with AC- O-500 cathode tested at 3 A g^{-1}

XPS was employed to analyze the chemical states of elements on the surface of the carbon samples. The full XPS spectrum (Fig. 5b) indicates that after oxidation, AC-O had the highest oxygen content (13.16%), which gradually decreased with the increase in the heat treatment temperature but was still higher than that of AC (5.97%). To further investigate the OFG components, fitting of the C 1s and O 1s spectra was carried out. The C 1s profiles (Fig. S5 a-e) show 4 fitted peaks at 284.8, 286.3, 287.5 and 289.1 eV, representing C—C/C=C, C—O, C=O and COO, respectively[54–56]. In the O 1s profiles (Fig. 5c-e and Table 2), the binding energies at about 531.3, 532.3, 533.3 and 534.3 eV are ascribed to C=O, OH, C—O—C and COO, respectively[57–58]. As shown in Fig. 5f, the OH content increases significantly after nitric acid oxidation, indicating that OH is mainly introduced during the oxidation process as previously reported[30, 59]. Additionally, the C=O and COO content increases slightly after nitric acid oxidation. Then, after thermal treatment at 500 °C, the reduction of O content is mainly attributed to the decrease in C—O

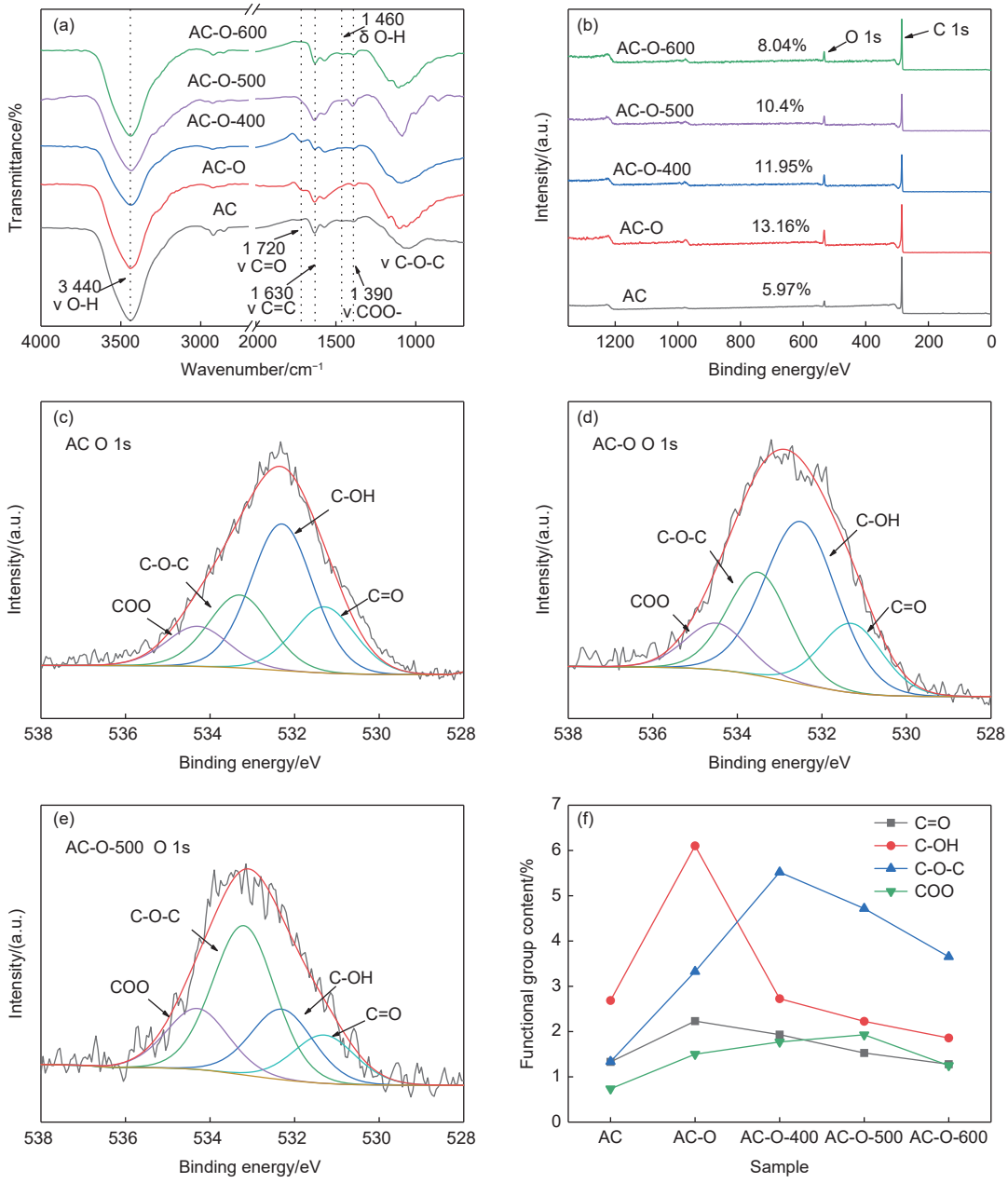

Fig. 5　(a) FTIR spectra, (b) XPS spectra, (c) O 1s spectra of AC, (d) AC-O, (e) AC-O-500 and (f) OFGs contents

Table 2　Analysis of the fitted O 1s peaks of the OFGs on the AC samples from XPS spectra

Samples	C=O (531.3 eV)/%	OH (532.3 eV)/%	C−O−C (533.3 eV)/%	COO (534.3 eV)/%
AC	1.33	2.69	1.34	0.74
AC-O	2.23	6.10	3.33	1.50
AC-O-400	1.93	2.73	5.52	1.77
AC-O-500	1.53	2.23	4.72	1.93
AC-O-600	1.28	1.86	3.65	1.25

content. Consequently, the COO content is further increased, which is consistent with the above FTIR spectra analysis. This reveals that dehydration condensation between hydroxyl groups occurs during the heat treatment process, leading to the formation of the carbon-oxygen double bond. Additionally, the distribution of OFGs is beneficial for increasing the capacitance. After heating to 600 °C, the thermally unstable OFGs at the carbon surface are removed, with only 8.04% of residual oxygen.

More than 50% of C—O content on the carbon surface constitute C—OH and C—O—C groups. According to previous reports, the hydroxyl group can improve the chemisorption of zinc ions and increase the reaction activity of C=O[60], thus improving the specific capacitance. As an electron-donating group, C—O—C facilitate pseudocapacitance and has high stability[61]. In AC-O-500, the synergistic effect between OFGs provides abundant pseudocapacitance, improves the electronegativity[62] and wettability of the carbon surface, and accelerates ions accumulation, thereby enhancing the capacitive performance.

Fig. 6a describes the changes of OFGs on the carbon surface during the oxidation and thermal treatment processes. Modified carbon sample, rich with OFGs such as —COO, has more reactive sites, which play a key role in increasing the capacitance. Additionally, OH and C—O—C also play a crucial role in the process of electrochemical energy storage. Fig. 6b depicts the Zn^{2+} storage mechanism of ZICs, which includes the ion adsorption/desorption of the EDLC energy storage process and the redox process by the introduction of the OFGs on the surface of AC[26, 37, 63]. Therefore, by tuning the types and number of OFGs, the wettability of the carbon cathode and the chemical adsorption of zinc ions were improved, leading to an increase in the specific capacitance and energy density of ZICs.

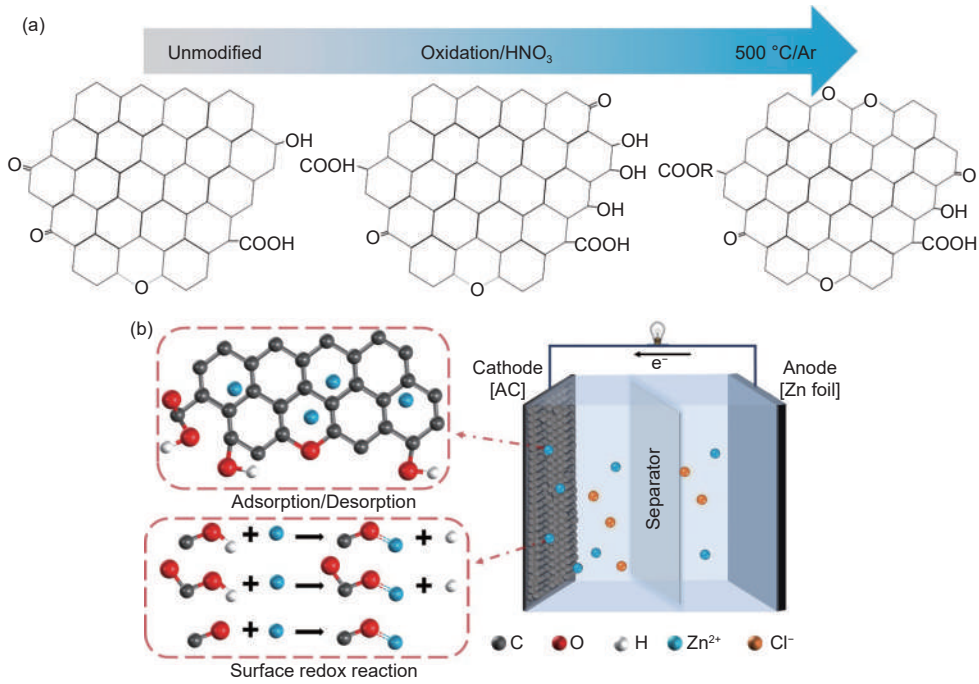

Fig. 6 (a) Schematic illustrations of the evolution of the OFGs under oxidation and thermal treatment and (b) ZIC energy storage mechanism

4 Conclusions

In this study, we demonstrated that by optimizing the OFGs at the carbon-based cathode surface, through nitric acid oxidation and thermal treatment, the capacitance of EtOH-based ZICs could be improved. At 1 A g^{-1}, the specific capacitance of the AC-O-500 sample was 195 F g^{-1}, which was 56% higher than that of pristine AC. AC-O-500 exhibited excellent stability, with more than 16 000 stable cycles, and maintained 100% coulombic efficiency at 3 A g^{-1}. FTIR and XPS analyses indicated that COO groups resulted in abundant electrochemically active sites, leading to highly reversible pseudocapacitance. This work provides important guidelines for optimizing OFGs in carbon materials for developing commercially viable ZICs and other energy storage devices.

Date availability statement

The data that support the findings of this study are openly available in Science Data Bank at https://

www.doi.org/10.57760/sciencedb.j00125.00013 or https://resolve.pid21.cn/31253.11.sciencedb.j00125.00013.

Acknowledgements

This work was financially supported by National Natural Science Foundation of China (52062012), Guangdong Province Key Discipline Construction Project (2021ZDJS102), the Innovation Team of Universities of Guangdong Province (2022KCXTD030, 2020KCXTD011), the Special Fund for Science and Technology Innovation Cultivation of Guangdong University Students (pdjh2023b0549) and the Student Academic Fund of Foshan University (xsjj202206kjb02).

Conflicts of interest

The authors declare no competing financial interest.

References

[1] Luo X Y, Chen S R, Hu T Z, et al. Renewable biomass-derived carbons for electrochemical capacitor applications[J]. SusMat, 2021, 1(2): 211-240.

[2] Zhai Y P, Dou Y Q, Zhao D Y, et al. Carbon materials for chemical capacitive energy storage[J]. Advanced Materials, 2011, 23(42): 4828-4850.

[3] Larcher D, Tarascon J M. Towards greener and more sustainable batteries for electrical energy storage[J]. Nature Chemistry, 2015, 7(1): 19-29.

[4] Tang H, Yao J J, Zhu Y R. Recent developments and future prospects for zinc-ion hybrid capacitors: a review[J]. Advanced Energy Materials, 2021, 11(14): 2003994.

[5] Wang H, Ye W, Yang Y, et al. Zn-ion hybrid supercapacitors: Achievements, challenges and future perspectives[J]. Nano Energy, 2021, 85: 105942.

[6] Li Z, Gadipelli S, Li H, et al. Tuning the interlayer spacing of graphene laminate films for efficient pore utilization towards compact capacitive energy storage[J]. Nature Energy, 2020, 5(2): 160-168.

[7] Dutta S, Bhaumik A, Wu K C W. Hierarchically porous carbon derived from polymers and biomass: effect of interconnected pores on energy applications[J]. Energy & Environmental Science, 2014, 7(11): 3574-3592.

[8] Zhi J, Zhao W, Liu X Y, et al. Highly conductive ordered mesoporous carbon based electrodes decorated by 3D graphene and 1D silver nanowire for flexible supercapacitor[J]. Advanced Functional Materials, 2014, 24(14): 2013-2019.

[9] Zou K, Cai P, Wang B, et al. Insights into enhanced capacitive behavior of carbon cathode for lithium ion capacitors: The coupling of pore size and graphitization engineering[J]. Nanomicro Letters, 2020, 12(1): 121.

[10] Liu Q Y, Zhang H Z, Xie J H, et al. Recent progress and challenges of carbon materials for Zn-ion hybrid supercapacitors[J]. Carbon Energy, 2020, 2(4): 521-539.

[11] Jin J, Geng X, Chen Q, et al. A better Zn-ion storage device: recent progress for Zn-ion hybrid supercapacitors[J]. Nanomicro Letters, 2022, 14(1): 64.

[12] Ma X P, Cheng J Y, Dong L B, et al. Multivalent ion storage towards high-performance aqueous zinc-ion hybrid supercapacitors[J]. Energy Storage Materials, 2019, 20: 335-342.

[13] Han P X, Xu G J, Han X Q, et al. Lithium ion capacitors in organic electrolyte system: scientific problems, material development, and key technologies[J]. Advanced Energy Materials, 2018, 8(26): 1801243.

[14] Dong L B, Yang W, Yang W, et al. Multivalent metal ion hybrid capacitors: A review with a focus on zinc-ion hybrid capacitors[J]. Journal of Materials Chemistry A, 2019, 7(23): 13810-13832.

[15] Wu S L, Chen Y T, Jiao T P, et al. An aqueous Zn-ion hybrid supercapacitor with high energy density and ultrastability up to 80000 cycles[J]. Advanced Energy Materials, 2019, 9(47): 1902915.

[16] Wang F, Borodin O, Gao T, et al. Highly reversible zinc metal anode for aqueous batteries[J]. Nature Materials, 2018, 17(6): 543-549.

[17] Hao J N, Li X L, Zeng X H, et al. Deeply understanding the Zn anode behaviour and corresponding improvement strategies in different aqueous Zn-based batteries[J]. Energy & Environmental Science, 2020, 13(11): 3917-3949.

[18] Yuan L B, Hao J N, Kao C C, et al. Regulation methods for the Zn/electrolyte interphase and the effectiveness evaluation in aqueous Zn-ion batteries[J]. Energy & Environmental Science, 2021, 14(11): 5669-5689.

[19] He Y, Zhuang X, Lei C, et al. Porous carbon nanosheets: Synthetic strategies and electrochemical energy related applications[J]. Nano Today, 2019, 24: 103-119.

[20] Luo X Y, Chen Y, Mo Y. A review of charge storage in porous carbon-based supercapacitors[J]. New Carbon Materials, 2021, 36(1): 49-68.

[21] Ao W, Fu J, Mao X, et al. Microwave assisted preparation of activated carbon from biomass: A review[J]. Renewable and Sustainable Energy Reviews, 2018, 92: 958-979.

[22] Luo X Y, Zheng H, Lai W D, et al. Defect engineering of carbons for energy conversion and storage applications[J]. Energy & Environmental Materials, 2023, 6: 1-22.

[23] Zheng Y W, Zhao W, Jia D D, et al. Porous carbon prepared via combustion and acid treatment as flexible zinc-ion capacitor electrode material[J]. Chemical Engineering Journal, 2020, 387: 124161.

[24] Wang Y G, Xia Y Y. Recent progress in supercapacitors: from

materials design to system construction[J]. Advanced Materials, 2013, 25(37): 5336-5342.

[25] Tang X N, Liu C Z, Chen X R, et al. Graphene aerogel derived by purification-free graphite oxide for high performance supercapacitor electrodes[J]. Carbon, 2019, 146: 147-154.

[26] Shao Y Y, Sun Z T, Tian Z N, et al. Regulating oxygen substituents with optimized redox activity in chemically reduced graphene oxide for aqueous Zn - ion hybrid capacitor[J]. Advanced Functional Materials, 2020, 31(6): 2007843.

[27] Lin Z Y, Liu Y, Yao Y G, et al. Superior capacitance of functionalized graphene[J]. The Journal of Physical Chemistry C, 2011, 115(14): 7120-7125.

[28] Hu P Y, Luo X Y, Hu T Z, et al. Ethanol solvent used in constructing ultra-low-temperature zinc ion capacitors with a long cycling life[J]. ACS Applied Materials & Interfaces, 2023, 15: 5180-5190.

[29] Sevilla M, Mokaya R. Energy storage applications of activated carbons: supercapacitors and hydrogen storage[J]. Energy & Environmental Science, 2014, 7(4): 1250-1280.

[30] Wu J P, Liu R R, Li M, et al. Boosting effects of hydroxyl groups on porous carbon for improved aqueous zinc-ion capacitors[J]. Journal of Energy Storage, 2022, 48: 103996.

[31] Raymundo-Piñero E, Kierzek K, Machnikowski J, et al. Relationship between the nanoporous texture of activated carbons and their capacitance properties in different electrolytes[J]. Carbon, 2006, 44(12): 2498-2507.

[32] Shi X, Zhang H Z, Zeng S Q S, et al. Pyrrolic-dominated nitrogen redox enhances reaction kinetics of pitch-derived carbon materials in aqueous zinc ion hybrid supercapacitors[J]. ACS Materials Letters, 2021, 3(9): 1291-1299.

[33] Zhang X R, Yang S, Jiang Y H, et al. Multi-dimensional graded electrodes with enhanced capacitance and superior cyclic stability[J]. Journal of Power Sources, 2021, 481: 228911.

[34] Li X R, Jiang Y H, Wang P Z, et al. Effect of the oxygen functional groups of activated carbon on its electrochemical performance for supercapacitors[J]. New Carbon Materials, 2020, 35(3): 232-243.

[35] Li J X, Han K H, Wang D, et al. Fabrication of high performance structural N-doped hierarchical porous carbon for supercapacitors[J]. Carbon, 2020, 164: 42-50.

[36] Zhong H M, Wang T T, Chen Y, et al. Understanding alkaline hydrogen evolution promoted by mesopores in three-dimensional graphene-like materials from perspective of capacitance effects[J]. Carbon, 2022, 199: 13-22.

[37] Zhang H Z, Liu Q Y, Fang Y B, et al. Boosting Zn-ion energy storage capability of hierarchically porous carbon by promoting chemical adsorption[J]. Advanced Materials, 2019, 31(44): 1904948.

[38] Li Y, Yang W, Yang W, et al. Towards high-energy and anti-self-discharge Zn-ion hybrid supercapacitors with new understanding of the electrochemistry[J]. Nanomicro Letters, 2021, 13(1): 95.

[39] Jiang Y Q, Liu J P. Definitions of pseudocapacitive materials: A brief review[J]. Energy & Environmental Materials, 2019, 2(1): 30-37.

[40] Yin J, Zhang W L, Wang W X, et al. Electrochemical zinc ion capacitors enhanced by redox reactions of porous carbon cathodes[J]. Advanced Energy Materials, 2020, 10(37): 2001705.

[41] Yang B J, Chen J T, Liu L Y, et al. 3D nitrogen-doped framework carbon for high-performance potassium ion hybrid capacitor[J]. Energy Storage Materials, 2019, 23: 522-529.

[42] Huo S, Zhao Y, Zong M, et al. Boosting supercapacitor and capacitive deionization performance of hierarchically porous carbon by polar surface and structural engineering[J]. Journal of Materials Chemistry A, 2020, 8(5): 2505-2517.

[43] Wang H, Wang M, Tang Y B. A novel zinc-ion hybrid supercapacitor for long-life and low-cost energy storage applications[J]. Energy Storage Materials, 2018, 13: 1-7.

[44] Zhang H Z, Fang Y B, Yang F, et al. Aromatic organic molecular crystal with enhanced π–π stacking interaction for ultrafast Zn-ion storage[J]. Energy & Environmental Science, 2020, 13(8): 2515-2523.

[45] Chen S M, Ma L T, Zhang K, et al. A flexible solid-state zinc ion hybrid supercapacitor based on co-polymer derived hollow carbon spheres[J]. Journal of Materials Chemistry A, 2019, 7(13): 7784-7790.

[46] Dong S Y, Shen L F, Li H S, et al. Flexible sodium-ion pseudocapacitors based on 3D $Na_2Ti_3O_7$ nanosheet arrays/carbon textiles anodes[J]. Advanced Functional Materials, 2016, 26(21): 3703-3710.

[47] Dong X L, Chen L, Su X L, et al. Flexible aqueous lithium-ion battery with high safety and large volumetric energy density[J]. Angewandte Chemie International Edition, 2016, 55(26): 7474-7477.

[48] Zeng Y X, Lin Z Q, Meng Y, et al. Flexible ultrafast aqueous rechargeable Ni//Bi battery based on highly durable single-crystalline bismuth nanostructured anode[J]. Advanced Materials, 2016, 28(41): 9188-9195.

[49] Wang Z Q, Zhou M, Qin L P, et al. Simultaneous regulation of cations and anions in an electrolyte for high-capacity, high-stability aqueous zinc-vanadium batteries[J]. eScience, 2022, 2(2): 209-218.

[50] Xiong D B, Li X F, Shan H, et al. Controllable oxygenic functional groups of metal-free cathodes for high performance lithium ion batteries[J]. Journal of Materials Chemistry A, 2015, 3(21): 11376-11386.

[51] Yuan S T, Huang X H, Wang H, et al. Structure evolution of oxygen removal from porous carbon for optimizing supercapacitor performance[J]. Journal of Energy Chemistry, 2020, 51: 396-404.

[52] Phattharasupakun N, Wutthiprom J, Suktha P, et al. High-performance supercapacitors of carboxylate-modified hollow carbon nanospheres coated on flexible carbon fibre paper: Effects of oxygen-containing group contents, electrolytes and operating temperature[J]. Electrochimica Acta, 2017, 238: 64-73.

[53] Ternero-Hidalgo J J, Rosas J M, Palomo J, et al. Functionalization of activated carbons by HNO_3 treatment: Influence of phosphorus

surface groups[J]. Carbon, 2016, 101: 409-419.

[54] Wang G M, Wang H Y, Lu X H, et al. Solid-state supercapacitor based on activated carbon cloths exhibits excellent rate capability[J]. Advanced Materials, 2014, 26(17): 2676-2682.

[55] Liu C, Wu J C, Zhou H, et al. Great enhancement of carbon energy storage through narrow pores and hydrogen-containing functional groups for aqueous Zn-ion hybrid supercapacitor[J]. Molecules, 2019, 24(14): 2589.

[56] Ha S H, Jeong Y S, Lee Y J. Free standing reduced graphene oxide film cathodes for lithium ion batteries[J]. ACS Applied Materials & Interfaces, 2013, 5(23): 12295-12303.

[57] Zou K Y, Cai P, Deng X L, et al. Highly stable zinc metal anode enabled by oxygen functional groups for advanced Zn-ion supercapacitors[J]. Chemical Communications, 2021, 57(4): 528-531.

[58] Chen C M, Zhang Q, Yang M G, et al. Structural evolution during annealing of thermally reduced graphene nanosheets for application in supercapacitors[J]. Carbon, 2012, 50(10): 3572-3584.

[59] Burgess R, Buono C, Davies P R, et al. The functionalisation of graphite surfaces with nitric acid: Identification of functional groups and their effects on gold deposition[J]. Journal of Catalysis, 2015, 323: 10-18.

[60] Sun T, Li Z J, Zhi Y F, et al. Poly(2, 5-Dihydroxy-1, 4-Benzoquinonyl Sulfide) as an efficient cathode for high-performance aqueous zinc-organic batteries[J]. Advanced Functional Materials, 2021, 31(16): 2010049.

[61] Lee J, Abbas M A, Bang J H. Exploring the capacitive behavior of carbon functionalized with cyclic ethers: A rational strategy to exploit oxygen functional groups for enhanced capacitive performance[J]. ACS Applied Materials & Interfaces, 2019, 11(15): 14126-14135.

[62] Wu K H, Wang D W, Gentle I R. Revisiting oxygen reduction reaction on oxidized and unzipped carbon nanotubes[J]. Carbon, 2015, 81: 295-304.

[63] Deng X Y, Li J J, Shan Z, et al. N, O co-doped hierarchical carbon cathode for high-performance Zn-ion hybrid supercapacitors with enhanced pseudocapacitance[J]. Journal of Materials Chemistry A, 2020, 8(23): 11617-11625.